NANO
LETTERS

xxxx
Vol. 0, No. 0
A−F

Enhanced Radiative Emission Rate and Quantum Efficiency in Coupled Silicon Nanocrystal-Nanostructured Gold Emitters

Julie S. Biteen,* Domenico Pacifici, Nathan S. Lewis, and Harry A. Atwater

California Institute of Technology, 1200 East California Boulevard, Pasadena, California 91125

Received June 25, 2005; Revised Manuscript Received July 28, 2005

ABSTRACT

We report local-field-enhanced light emission from silicon nanocrystals close to a film of nanoporous gold. We resolve photoluminescence as the gold–Si nanocrystal separation distance is varied between 0 and 20 nm and observe a fourfold luminescence intensity enhancement concomitant with increases in the coupled silicon nanocrystal/nanoporous gold absorbance cross section and radiative decay rate. A detailed analysis of the luminescence data indicated a local-field-enhanced quantum efficiency of 58% for the Si nanocrystals coupled to the nanoporous gold layer.

Since the discovery of strong room-temperature photoluminescence from porous silicon in 1990,[1,2] considerable effort has been devoted to the development of silicon-based optoelectronics for integrated photonics, an integral part of which is a long-sought Si-based power efficient light emitter. Silicon nanostructures have been investigated intensively as light emission sources. They have been made by many different methods, including porous etching,[1] implantation of Si^+ ions,[3] aerosol synthesis,[4] rf cosputtering of Si and SiO_2,[5] and chemical vapor deposition of SiO and SiO_2.[6] These materials exhibit efficient luminescence because of the radiative emission of long-lived quantum-confined excitons in silicon nanocrystals (nc-Si), which emit in the near-infrared to visible range because of an increase in the exciton emission energy relative to bulk silicon.[7] Emission from Si nanocrystals has been studied in various systems, from single nanocrystals[8] to multilayered structures,[9] and efficient electroluminescence[10−12] and high gain values[13,14] have been reported.

As light-emitters, silicon nanocrystals have many desirable properties. They exhibit room-temperature luminescence with high quantum efficiencies, and the emission energy can be tuned throughout the visible range by varying the nanocrystal size[15] or surface termination.[16] However, because of the indirect band gap, nc-Si suffers from a low radiative emission rate and a small absorbance cross section, which decreases the photoluminescence (PL) intensity relative to direct band gap semiconductors and organic dyes. A method for overcoming this specific limitation is thus highly desirable. It has been observed in compound semiconductor materials that coupling to a metal can lead to enhanced emission from solid-state quantum dots[17,18] and wells.[19]

In this paper, we show first evidence of PL enhancement from nc-Si coupled to metal nanostructures and report on a separation-distance-resolved study of radiative decay rate, effective absorbance cross section, and quantum efficiency, as well as PL intensity for the coupled emitter−nanostructured metal system.

Si nanocrystals were produced by ion implantation of 11 keV Si^+ ions to a fluence of 1.7×10^{16} cm^{-2} into a 1.6-mm-thick fused quartz strip (Technical Glass Products). According to Monte Carlo simulations performed with SRIM,[20] such an implantation yields a Gaussian depth distribution of Si in the SiO_2, with a peak excess Si concentration of 10% at a depth of ∼20 nm. The implanted quartz was annealed in argon for 20 min at 200 °C and 20 min at 450 °C to dry the surface and then again for 30 min at 1000 °C to form nc-Si. The samples were subsequently heated in 10% hydrogen in nitrogen forming gas ambient for 30 min at 450 °C to eliminate emission from defect states in the SiO_2 matrix.[21]

After nc-Si formation, the surface of the 9-cm-long strip of nc-Si-doped quartz sample was etched in a 1:20 mixture of 48% HF in water in a stepwise fashion. The etch rate was 0.25 nm/s, precisely calibrated by spectral ellipsometry (Sentech SE-850) of an analogous sample of SiO_2 on a Si substrate. Nine 2.5-nm steps were etched using a stepper motor to control for step length (1 cm) and etch time (10 s). Each step was uniform within ±0.2 nm across the majority

* Corresponding author. E-mail: jsbiteen@caltech.edu; tel: 626-395-3826; fax: 626-844-9320.

10.1021/nl051207z CCC: $30.25
Published on Web 00/00/0000

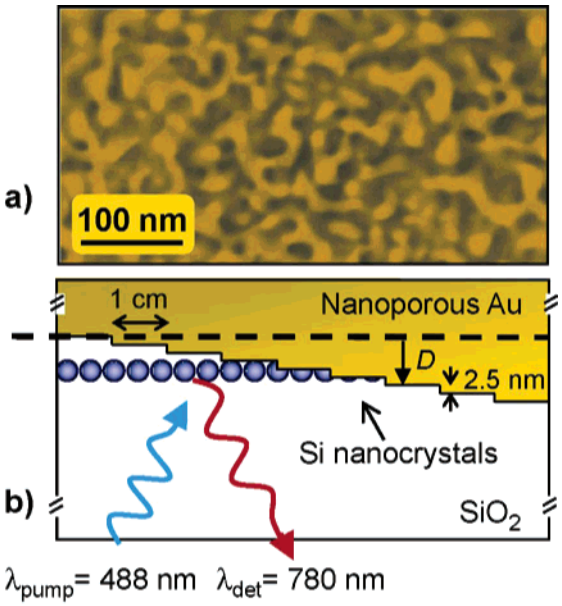

Figure 1. (a) False color plan view (100 K magnification) SEM of the nanoporous gold surface showing features on the order of 10 nm. (b) Schematic cross section of the sample. PL measurements are made from the bottom side of all samples.

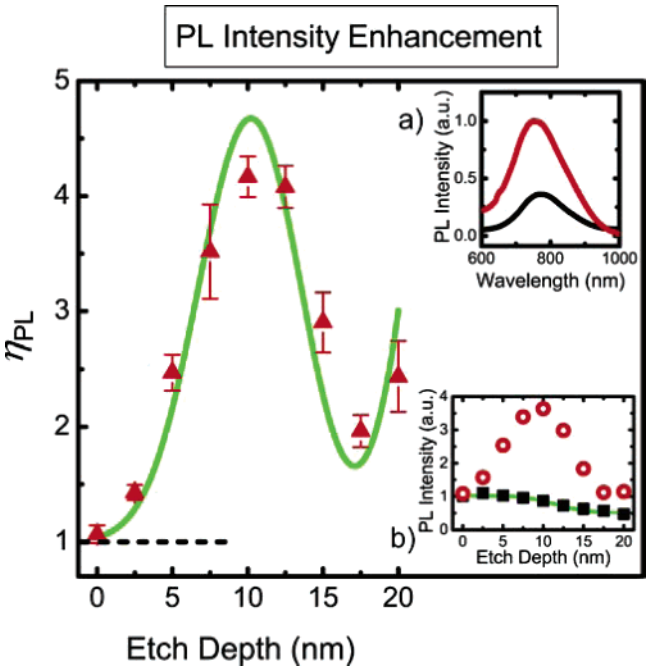

Figure 2. PL intensity enhancement, η_{PL}, measured at 780 nm as a function of etch depth, D (triangles). The solid line is a fit to the data using a model that accounts for the spatial distribution of Si nanocrystals and the enhanced local-field. Insets: (a) Typical PL spectra for the reference (black) and coupled np-Au/nc-Si (red) samples, at $D = 5$ nm. (b) PL intensities at 780 nm vs etch depth for the reference (squares) and coupled np-Au/nc-Si (circles) samples. The reference intensities are well fit by the green line, which is the integral of two Gaussian distributions that peak at 14.2 and 24.2 nm, respectively.

of its length. The 9-cm strip of nc-Si at different depths was then split lengthwise in two, and the first half was retained as a reference sample.

Subsequently, a film of nanoporous gold was prepared according to a method developed by Erlebacher and co-workers.[22] A 100-nm-thick 12-carat gold leaf (50:50 Au/Ag alloy; Sepp Leaf Products) was dealloyed in 70% nitric acid for 10 min, whereby the selective dissolution of Ag left behind a nanoporous Au (np-Au) film, 150-nm-thick and found to be composed of approximately 50% Au and 50% voids. As shown in the scanning electron micrograph of Figure 1a, obtained by using a LEO 1550VP Field Emission SEM, the gold feature dimensions are on the order of 10 nm and range from spheres to prolate spheroids with aspect ratios up to ~1:3. The so-formed nanoporous gold layer was then adhered to the quartz surface. Therefore, at each step in the coupled sample, the np-Au was brought 2.5 nm closer to the center of the nc-Si distribution, as schematized in Figure 1b.

Photoluminescence (PL) spectra were acquired under excitation from the $\lambda_{ex} = 488$ nm line of an Ar^+ laser focused to a 1-mm^2 spot. The PL intensity was measured using a charge-coupled device detector (sensitivity range 200−1100 nm), cooled with liquid nitrogen to −132 °C, in conjunction with a 27.5-cm focal length grating spectrograph. A dichroic filter that cuts off wavelengths below 510 nm was used to eliminate scattered laser light from the measurements. Time-resolved PL measurements were performed by chopping the 488-nm excitation source with an acousto-optic modulator at a frequency of 250 Hz, and this PL was recorded with a GaAs photomultiplier tube in conjunction with a multichannel photon counting system. The time resolution of the system was ≤50 ns. PL measurements were made through the transparent side of the samples, as indicated by the arrows at the bottom of Figure 1b, and the reference sample was laid nanocrystal-side down on a polished silicon substrate to account for any reflection effects in the coupled np-Au/nc-Si sample.

Typical PL spectra from the reference and np-Au/nc-Si samples are reported in inset a of Figure 2 (black and red lines, respectively) for an etch depth, $D = 5$ nm, and for an excitation power density, $P_{ex} = 50$ mW/mm^2. The PL intensity of the coupled sample is enhanced and slightly blue-shifted with respect to the reference sample. To better understand the origin of this PL enhancement, we fixed the detection wavelength at 780 nm, thus focusing our investigation on a precise Si nanocrystal size because nc-Si PL is size-dependent. In inset b of Figure 2, the PL intensities measured at 780 nm for both the reference (squares) and the np-Au/nc-Si coupled sample (circles) are reported as a function of D.

The Gaussian Si^+ ion implantation profile used to produce the nc-Si sample has been observed previously to give a Gaussian distribution of nc-Si concentrations in which larger nanocrystals are abundant at the center of the Gaussian and smaller nanocrystals lie mainly in the tails.[23] Measurements of the reference sample PL intensity integrated over all wavelengths as a function of D (not shown) indicated that the center of the nc-Si distribution is 19.2 ± 0.1 nm from the unetched surface. Because the variations in emission wavelength as a function of etch depth were small, we assumed the emitter oscillator strength to be roughly constant throughout the sample, and thereby found the emission as a

function of depth to be consistent with a Gaussian distribution of width of 14.0 ± 0.2 nm. Within this ensemble, Si nanocrystals emitting at 780 nm are of an intermediate size, and are therefore expected to have a bimodal concentration profile about the center at 19.2 nm. The squares in inset b of Figure 2 show the dependence of the PL intensity of the reference sample, I_{PLref}, on D. The green line beneath these data shows that they are well fit by the integral of two Gaussian distributions, peaking at 14.2 and 24.2 nm, respectively. The etch depth, D, is therefore a measure of the np-Au/nc-Si separation distance.

We define the photoluminescence (PL) intensity enhancement, $\eta_{PL}(D)$ at depth D, as the ratio between the PL intensity of the np-Au/nc-Si coupled sample, $I_{PLnpg}(D)$, and $I_{PLref}(D)$, that is, $\eta_{PL}(D) = I_{PLnpg}(D)/I_{PLref}(D)$. This enhancement is reported in Figure 2 (solid triangles) for $P_{ex} = 50$ mW/mm^2. Interestingly, the PL intensity enhancement is >1 for all the etching depths and reaches a fourfold maximum peak at $D = 10$ nm. It is therefore clear that the presence of the np-Au layer in proximity to the nc-Si plays a crucial role in determining the optical properties of the emitting centers. To understand the physical origin of the increase in luminescence intensity, we begin by noticing that, for a given photon flux, ϕ, the PL intensity of N optically active emitting centers is directly proportional to the product of the number of excited centers, N^*, and the radiative decay rate, Γ_{rad}. In particular, under steady-state conditions, an analysis of the two-level system yields

$$I_{PL} \propto N^*\Gamma_{rad} = \frac{\sigma\phi}{\sigma\phi + \Gamma_{exp}} N\Gamma_{rad} \quad (1)$$

where σ is the excitation cross section, and the experimental decay rate, $\Gamma_{exp} = \Gamma_{rad} + \Gamma_{nr}$, comprises the radiative as well as the nonradiative de-excitation paths. In the low excitation regime, eq 1 reduces to

$$I_{PL} \propto N\frac{\sigma\phi}{\Gamma_{exp}}\Gamma_{rad} \qquad (\sigma\phi \ll \Gamma_{exp}) \quad (2)$$

which indicates that, for a fixed number of optically active centers and a constant photon flux, the PL intensity depends on measurable physical quantities such as σ and Γ_{exp}, as well as on the radiative emission rate, Γ_{rad}, whose value is mostly unknown. Because, for a given etch depth, ϕ and N are identical for both the reference and the np-Au/nc-Si coupled samples, the PL intensity enhancement, $\eta_{PL}(D)$, can be decomposed by using eq 2 as follows:

$$\eta_{PL} = \frac{I_{PLnpg}}{I_{PLref}} = \frac{\sigma_{npg}}{\sigma_{ref}}\frac{\Gamma_{rad-npg}}{\Gamma_{rad-ref}}\frac{\Gamma_{exp-ref}}{\Gamma_{exp-npg}} = \frac{\eta_\sigma\eta_{\Gamma_{rad}}}{\eta_{\Gamma_{exp}}} \quad (\sigma\phi \ll \Gamma_{exp}) \quad (3)$$

Here, $\eta_\sigma(D) = \sigma_{npg}(D)/\sigma_{ref}(D)$, $\eta_{\Gamma_{rad}}(D) = \Gamma_{rad-npg}(D)/\Gamma_{rad-ref}(D)$, and $\eta_{\Gamma_{exp}}(D) = \Gamma_{exp-npg}(D)/\Gamma_{exp-ref}(D)$ are the enhancements in the effective excitation cross section, radiative decay rate, and experimental decay rate, respectively, at etch depth D.

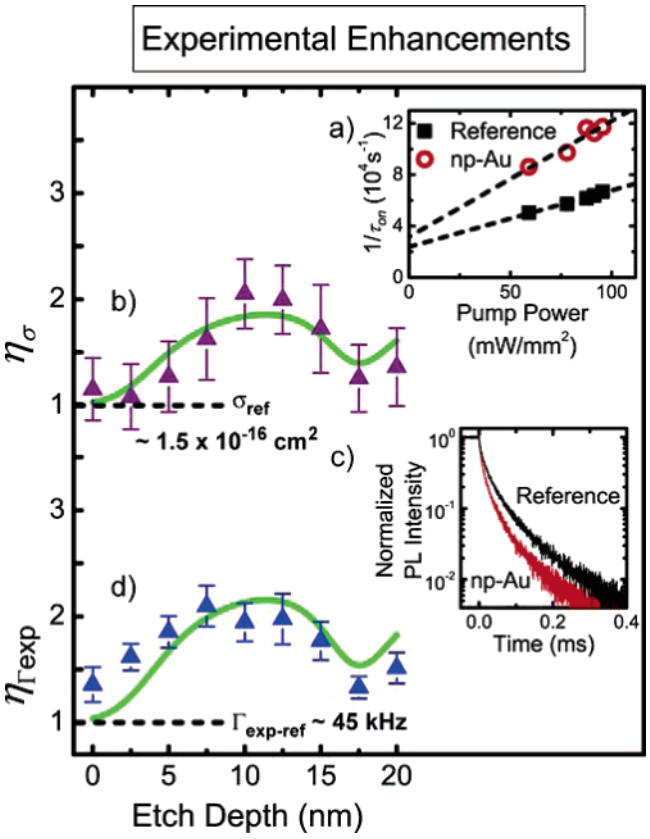

Figure 3. (a) Representative values of turn on rate as a function of pump power (at $D = 10$ nm) that were used in eq 4 to calculate the absorbance cross sections for the reference (solid squares) and coupled (open circles) samples. (b) Effective excitation cross section enhancement, η_σ, at 780 ± 20 nm. (c) Representative PL decay traces for the reference (black) and coupled np-Au/nc-Si (red) samples at $D = 10$ nm. (d) Experimental decay rate enhancement, $\eta_{\Gamma_{exp}}$, at 780 ± 20 nm. The solid lines in b and d are fits to the data using a model that accounts for the spatial distribution of Si nanocrystals and the enhanced local-field.

The effective excitation cross sections of the reference and coupled np-Au/nc-Si samples, σ_{ref} and σ_{npg}, were determined from measurements of the PL rise time at $\lambda_{det} = 780 \pm 20$ nm with a technique derived from the steady-state relationships present above.[24,25] The rise time, τ_{on}, defined as the average $1/e$ time for the PL intensity to reach its saturation value, is inversely related to σ, according to the expression

$$1/\tau_{on} = \sigma\phi + \Gamma_{exp} \quad (4)$$

The turn on rate, $\Gamma_{on} = \tau_{on}^{-1}$, was measured as a function of the photon flux, ϕ, in the reference and np-Au/nc-Si samples at each D; the results for $\Gamma_{on}(D = 10$ nm) are shown in inset a of Figure 3 for the reference (squares) and coupled (circles) samples. The $\sigma(D)$ is determined from the slope of this graph; σ_{ref} was found to be essentially constant at ~1.5 × 10^{-16} cm^2, whereas $\sigma_{npg}(D)$ was highly dependent on D and always greater than or equal to $\sigma_{ref}(D)$. The purple triangles reported in Figure 3b show the excitation cross section enhancement, $\eta_\sigma(D)$, as a function of etch depth, D. The peak value is greater than 2 at $D = 10-12.5$ nm, meaning that the effective excitation cross section for the

nc-Si emitting at 780 nm is enhanced by a factor of 2 in the presence of the np-Au layer. This enhancement alone, however, cannot account for the fourfold increase in PL intensity of Figure 2. Therefore, according to eq 3, either Γ_{exp} or Γ_{rad} (or both) must also be affected by the np-Au layer.

Inset c of Figure 3 shows representative curves for the experimental PL decay of both samples at $D = 10$ nm. The PL intensity for the np-Au/nc-Si sample decays faster than the reference sample, as was found to be true at all etch depths. In particular, the reference sample is characterized by an experimental decay rate, $\Gamma_{exp-ref} = 40-50$ kHz, that is only weakly dependent on D. However, the PL decay rate for the np-Au/nc-Si sample is highly dependent on D, its values varying in the range 55−105 kHz. The blue triangles in Figure 3d show the experimental decay rate enhancement, $\eta_{\Gamma_{exp}}(D)$, as a function of D. This ratio is greater than unity for all D, and it reaches its maximum (∼2) at 7.5 nm $< D <$ 12.5 nm. Interestingly, the enhancement of experimental decay rate roughly equals the increase in excitation cross section, in such a way that the two cancel each other out in eq 3, giving as a result no net contribution to the PL intensity enhancement. Therefore, to explain the experimentally observed fourfold PL intensity increase, we deduce that the nc-Si radiative emission rate, Γ_{rad}, must also increase in the vicinity of an np-Au film.

We measured Γ_{exp} at $P_{ex} = 50$ mW/mm^2, and σ was calculated using values of τ_{on} acquired at $5 < P_{ex} < 100$ mW/mm^2. At these pump powers, $\sigma\phi \cong 10^2-10^3$ s$^{-1} \ll \Gamma_{exp} \cong 5 \times 10^4$ s^{-1}. Thus we use eq 3, together with the measured enhancements η_{PL}, η_σ, and $\eta_{\Gamma_{exp}}$ reported in Figures 2 and 3, to directly estimate $\eta_{\Gamma_{rad}}$ for the nc-Si emitting at 780 ± 20 nm. The results are reported as inverted triangles in Figure 4. The enhancement $\eta_{\Gamma_{rad}}$ depends strongly on D, in particular it is greater than unity at all separation distances with a peak of ∼4.5 at $D = 7.5$ nm. Indeed, this behavior suggests that the increase in radiative decay rate reported in Figure 4 is uniquely responsible for the observed enhancement in PL intensity in Figure 2.

On the basis of this analysis, it is possible to give a quantitative estimate of the absolute values of the radiative rate, and therefore the quantum efficiency of the nc-Si system. The enhancement in quantum efficiency, $\eta_{QE} = QE_{npg}/QE_{ref}$ is a function of the decay rate enhancements.

$$\eta_{QE} = \frac{QE_{npg}}{QE_{ref}} = \frac{\Gamma_{rad-npg}}{\Gamma_{exp-npg}}\frac{\Gamma_{exp-ref}}{\Gamma_{rad-ref}} = \frac{\eta_{\Gamma_{rad}}}{\eta_{\Gamma_{exp}}} \quad (5)$$

The inverted triangles in Figure 5 show η_{QE}, as calculated from eq 5, using the data for $\eta_{\Gamma_{rad}}$ and $\eta_{\Gamma_{exp}}$ reported in Figures 4 and 3d. The enhancement in quantum efficiency is dependent on D and has a peak of ∼2 for 5 nm $< D <$ 12.5 nm.

From the definitions of the radiative and experimental rate enhancements, it follows that

$$\eta_{\Gamma_{rad}} = \eta_{\Gamma_{exp}}\left(\frac{\Gamma_{exp-ref}}{\Gamma_{rad-ref}}\right) - \left(\frac{\Gamma_{nr-npg}}{\Gamma_{rad-ref}}\right) \quad (6)$$

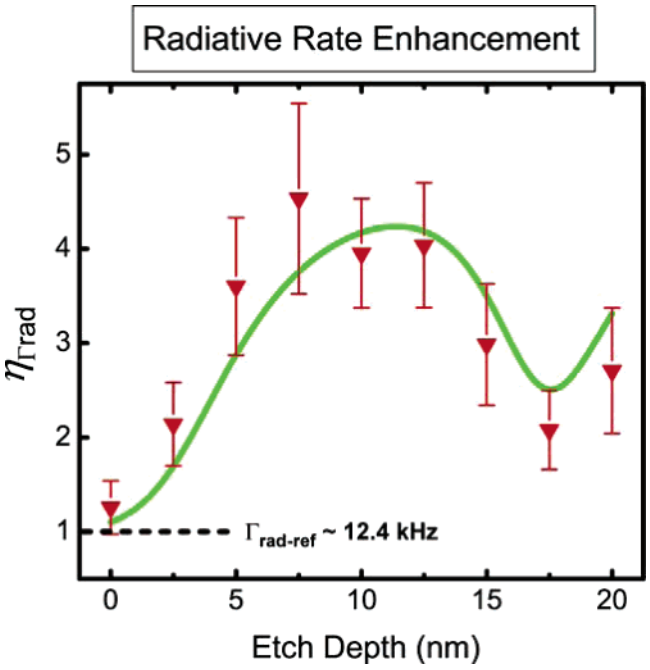

Figure 4. Radiative decay rate enhancement, $\eta_{\Gamma_{rad}}$, calculated with eq 3 for nc-Si emitting at 780 nm coupled to the np-Au film. The solid line is a fit to the data using a model that accounts for the spatial distribution of Si nanocrystals and the enhanced local-field.

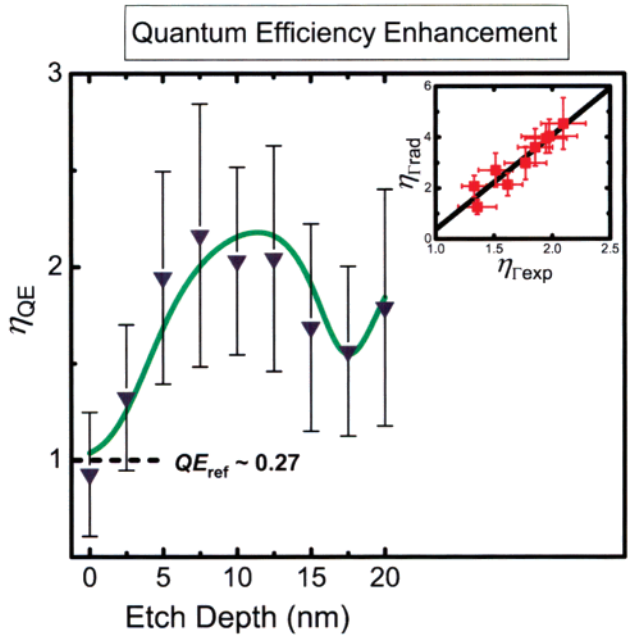

Figure 5. Quantum efficiency enhancement, η_{QE}, for nc-Si emitting at 780 nm and coupled to the np-Au film, as calculated using eq 5. The solid line is a fit to the data using a model that accounts for the spatial distribution of Si nanocrystals and the enhanced local-field. Inset: The decay rate enhancements, $\eta_{\Gamma_{rad}}$ and $\eta_{\Gamma_{exp}}$, are compared and fit to a straight line (reduced $\chi^2 = 0.14$) as in eq 6, to extract the slope, $(\Gamma_{exp-ref}/\Gamma_{rad-ref}) = 3.70 \pm 0.90$, from which a quantum efficiency of 27% can be derived for the reference sample, and the y intercept, $(-\Gamma_{nr-npg}/\Gamma_{rad-ref}) = -3.33 \pm 0.82$.

Here, Γ_{nr-npg} is the nonradiative decay rate of the coupled sample. Because for the reference sample $\Gamma_{exp-ref} = \Gamma_{rad-ref} + \Gamma_{nr-ref}$ is constant as a function of etch depth D, we can reasonably assume that $\Gamma_{rad-ref}$ and Γ_{nr-ref} are also constant.

Moreover, assuming that Γ_{nr-npg} is also approximately constant with D, a plot of $\eta_{\Gamma_{rad}}$, shown in Figure 4, versus $\eta_{\Gamma_{exp}}$, reported in Figure 3d, should give a straight line, according to eq 6. In the inset of Figure 5, the experimental values of $\eta_{\Gamma_{rad}}$ and $\eta_{\Gamma_{exp}}$ are reported in a scatter graph. The trend is clearly linear, and indeed the data are very well fit (reduced $\chi^2 = 0.14$) by a straight line with slope, $(\Gamma_{exp-ref}/\Gamma_{rad-ref}) = 3.70 \pm 0.90$, and y intercept, $(-\Gamma_{nr-npg}/\Gamma_{rad-ref}) = -3.33 \pm 0.82$. From the slope, and the measured $\Gamma_{exp-ref} \approx 45$ kHz, we find for the reference sample that $\Gamma_{rad-ref} \approx 12.4$ kHz, as indicated by the dashed line in Figure 4. This measurement, corresponding to a radiative lifetime of 80 μs, is in good agreement with the values estimated by Garcia and co-workers[26] and within the range calculated by Delerue et al.[27] The value of QE_{ref} for the reference sample is the inverse of the slope, that is, 27%, as indicated by the dashed line in Figure 5. From this value and the values of η_{QE} in Figure 5, we estimate a peak enhanced quantum efficiency of 58% for nc-Si coupled to the nanoporous gold layer.

The enhancements observed in Figures 2−5 can be explained by considering the geometry of the system. Small gold particles will strongly concentrate electric fields,[28] so an enhanced local field is present about the ellipsoids and spheroids that make up the np-Au film. A silicon nanocrystal in this enhanced field will have an altered optical density of states, and steady-state analysis indicates that this will enhance the decay rate of the nc-Si.[29] Additionally, np-Au is strongly absorbing over a broad range of wavelengths, and can therefore act as a sensitizer for nc-Si in its local field. Finally, the roughness on the surface of the np-Au contains a wide array of spatial frequencies, allowing any nc-Si emission energy transferred to a surface plasmon at the np-Au/SiO_2 interface to be coupled out into the radiation field.

The dependences of the enhancements, η_{PL}, η_{σ}, $\eta_{\Gamma_{exp}}$, $\eta_{\Gamma_{rad}}$ and η_{QE}, on etch depth, D, as shown in Figures 2−5 are all nonmonotonic. These enhancements peak at 7.5 nm < D < 12.5 nm, and have a rising tail at $D = 17.5-20$ nm. Our results can be interpreted in the context of a model that accounts for local-field effects as well as the spatial distribution of nanocrystals in the sample. The nanocrystals closest to the np-Au will be most affected by its presence because the strength of the enhanced local field is expected to decay with metal/emitter separation distance, r, as r^{-6}. At extremely small nc-Si/np-Au separations, however, luminescence quenching processes must be considered,[30] and if np-Au directly contacts a Si nanocrystal, electronic charge transfer could also quench luminescence.[11] The green lines in Figures 2−5 are fits produced by applying such a model to our data.

In conclusion, coupling Si nanocrystals to nanoporous gold yields a fourfold enhancement in PL intensity at 780 nm, which was shown to be related to the fourfold enhancement in radiative decay rate as a result of local-field effects. The effective excitation cross section and quantum efficiency are enhanced by a factor of 2. These enhancements are especially promising considering that, here with a wide distribution of nc-Si, they contain contributions from a large number of unenhanced nanocrystals at large separation distances, which limits the overall achievable emission enhancement. Also, most nanocrystals are nonresonant with the np-Au in the present work. Despite the complex structure of the nanoporous gold, the model developed here shows a close correspondence to the experimental data, and this fit indicates that with an optimized nanostructured sample consisting of a single, uniform (straggle ≤ 1 nm) monolayer of nc-Si resonant with np-Au, we can envisage enhancements in radiative decay rate, absorbance cross section, and quantum efficiency, and therefore in PL intensity, by as much as 2 orders of magnitude. Such an increase in the Si nanocrystal emission rate can make nc-Si competitive with direct band gap light emitters and enable the fragmentation of brighter nc-Si LEDs, and possibly allow high optical gain in an all-silicon device fabrication processes.

Acknowledgment. This work was partially supported by NSF Grant CHE-0213589.

Supporting Information Available: Measurements of the absorbance cross sections of the np-Au film and nc-Si emitters, as well as a discussion of the enhancement in PL intensity integrated over all detection wavelengths and its dependence on pump power, can be found in the Supporting Information section. This material is available free of charge via the Internet at http://pubs.acs.org.

References

(1) Canham, L. T. *Appl. Phys. Lett.* **1990**, *57*, 1046−1048.
(2) Cullis, A. G.; Canham, L. T. *Nature* **1991**, *353*, 335−338.
(3) Shimizu-Iwayama, T.; Nakao, S.; Saitoh, K. *Appl. Phys. Lett.* **1994**, *65*, 1814−1816.
(4) Brus, L. E.; Szajowski, P. F.; Wilson, W. L.; Harris, T. D.; Schuppler, S.; Citrin, P. H. *J. Am. Chem. Soc.* **1995**, *117*, 2915−2922.
(5) Zhang, Q.; Bayliss, S. C.; Hutt, D. A. *Appl. Phys. Lett.* **1995**, *66*, 1977−1979.
(6) Zacharias, M.; Heitmann, J.; Scholz, R.; Kahler, U.; Schmidt, M.; Blasing, J. *Appl. Phys. Lett.* **2002**, *80*, 661−663.
(7) Delley, B.; Steigmeier, E. F. *Phys. Rev. B* **1993**, *47*, 1397−1400.
(8) Valenta, J.; Juhasz, R.; Linnros, J. *Appl. Phys. Lett.* **2002**, *80*, 1070−1072.
(9) Lu, Z. H.; Lockwood, D. J.; Baribeau, J. M. *Nature* **1995**, *378*, 258−260.
(10) Lalic, N.; Linnros, J. *J. Lumin.* **1998**, *80*, 263−267.
(11) Walters, R. J.; Bourianoff, G. I.; Atwater, H. A. *Nat. Mater.* **2005**, *4*, 143−146.
(12) Irrera, A.; Pacifici, D.; Miritello, M.; Franzò, G.; Priolo, F.; Iacona, F.; Sanfilippo, D.; Di Stefano, G.; Fallica, P. G. *Appl. Phys. Lett.* **2002**, *81*, 1866−1868.
(13) Pavesi, L.; Dal Negro, L.; Mazzoleni, C.; Franzò, G.; Priolo, F. *Nature* **2000**, *408*, 440−444.
(14) Ruan, J.; Fauchet, P. M.; Dal Negro, L.; Cazzanelli, M.; Pavesi, L. *Appl. Phys. Lett.* **2003**, *83*, 5479−5481.
(15) Fischer, T.; Petrova-Koch, V.; Shcheglov, K.; Brandt, M. S.; Koch, F. *Thin Solid Films* **1996**, *276*, 100−103.
(16) Wolkin, M. V.; Jorne, J.; Fauchet, P. M.; Allan, G.; Delerue, C. *Phys. Rev. Lett.* **1999**, *82*, 197−200.
(17) Shimizu, K. T.; Woo, W. K.; Fisher, B. R.; Eisler, H. J.; Bawendi, M. G. *Phys. Rev. Lett.* **2002**, *89*, 117401.
(18) Kulakovich, O.; Strekal, N.; Yaroshevich, A.; Maskevich, S.; Gaponenko, S.; Nabiev, I.; Woggon, U.; Artemyev, M. *Nano Lett.* **2002**, *2*, 1449−1452.
(19) Okamoto, K.; Niki, I.; Shvartser, A.; Narukawa, Y.; Mukai, T.; Scherer, A. *Nat. Mater.* **2004**, *3*, 601−605.

(20) Ziegler, J. F.; Biersack, J. P.; Littmark, U. *The Stopping and Range of Ions in Solids*; Pergamon Press: New York, 1985.
(21) Min, K. S.; Shcheglov, K. V.; Yang, C. M.; Atwater, H. A.; Brongersma, M. L.; Polman, A. *Appl. Phys. Lett.* **1996**, *68*, 2511−2513.
(22) Ding, Y.; Erlebacher, J. *J. Am. Chem. Soc.* **2003**, *125*, 7772−7773.
(23) Brongersma, M. L.; Polman, A.; Min, K. S.; Atwater, H. A. *J. Appl. Phys.* **1999**, *86*, 759−763.
(24) Kovalev, D.; Diener, J.; Heckler, H.; Polisski, G.; Kunzner, N.; Koch, F. *Phys. Rev. B* **2000**, *61*, 4485−4487.
(25) Franzò, G.; Coffa, S.; Priolo, F.; Spinella, C. *J. Appl. Phys.* **1997**, *81*, 2784−2793.
(26) Garcia, C.; Garrido, B.; Pellegrino, P.; Ferre, R.; Moreno, J. A.; Morante, J. R.; Pavesi, L.; Cazzanelli, M. *Appl. Phys. Lett.* **2003**, *82*, 1595−1597.
(27) Delerue, C.; Allan, G.; Lannoo, M. *Phys. Rev. B* **1993**, *48*, 11024−11036.
(28) Bohren, C. F.; Huffman, D. R. *Absorption and Scattering of Light by Small Particles*; John Wiley & Sons: New York, 1983.
(29) Gersten, J.; Nitzan, A. *J. Chem. Phys.* **1981**, *75*, 1139−1152.
(30) Tchebotareva, A. L.; de Dood, M. J. A.; Biteen, J. S.; Atwater, H. A.; Polman, A. *J. Lumin.* **2005**, *114*, 137−144.

NL051207Z